# OPTICAL FREEZE-FRAMING AND ANALYSIS OF NANOFLUIDIC BEHAVIORS IN ELASTOMERIC NANOCAVITIES

Myung Gi Ji<sup>1</sup>, Qiang Li<sup>1</sup>, and Jaeyoun (Jay) Kim<sup>1,2,\*</sup>

<sup>1</sup>Department of Electrical & Computer Engineering, Iowa State University, Ames, Iowa, USA <sup>2</sup>Microelectronics Research Center, Iowa State University, Ames, Iowa, USA

# **ABSTRACT**

The behavior of liquid-phase polymer in nanoscale cavities are essential and important to many technological processes. The level of our understanding on them, however, is still limited. This paper reports a new photofluidic technique to capture, or "freeze-frame", the capillary rise of polymer into elastomeric nanocavities with nanoscopic resolutions and reveals nonlinear and unstable natures of the polymeric capillary effect. Based on the results, a nanofluidic model is also proposed to explain the anomalies. Both the freeze-framing technique and the established model will open new pathways to analyze and utilize nanofluidics.

## **KEYWORDS**

Capillary Effect, Capillary Force Lithography, Nanocapillarity, Nanofluidics, Nanoimprinting

## INTRODUCTION

Capillary filling of nanoscale cavities with polymeric fluids is ubiquitous in many nanoscale processes. One prominent example is the important technique of capillary force lithography (CFL) [1]. To date, however, how the polymeric fluids interact with nanoscale cavities and in what fashion the capillary rise progresses along the cavity wall were not known in detail. The reason was simple – Lack of effective means to observe the capillary rise with sufficient temporal and spatial resolutions. This work attempts to capture, or "freeze-frame", the progress of the capillary rise with sub-10-nm-scale height increment using photofluidic control. This new technique not only enables

high-precision monitoring of the capillary rise but also leads to a novel method to print nanoscale pillars with different heights as a function of position.

## **EXPERIMENTAL METHODS**

# **Capillary Action of Photopolymer in PDMS Cavities**

Figure 1 describes our photofluidic "freeze-framing" process. It is very similar to the standard CFL process, except for the addition of the UV pre-curing process (Fig. 1b) which enables nanoscopic volume control of the photopolymer. The array of nanocavities, which will be used as the nanoscale capillaries for liquid-phase polymer later, was realized via replica-molding of a commercially available silicon nanopost array with hard PDMS (*h*-PDMS). As the liquid-phase photopolymer, which will be "frozen" by a blanket of UV illumination for fixating the shape, the optical adhesive NOA73 was chosen for its wide availability and excellent chemical, optical, and mechanical properties.

As shown in Fig. 2, UV-induced solidification of photopolymer starts from the inner volume, not from the top surface, due to the oxygen inhibition effect. So, the UV pre-curing produces a layer of liquid photopolymer which becomes increasingly thinner with the UV-dose. By controlling the UV-dose, we can control the volume of the "liquid" photopolymer available for the capillary rise. At the completion of the capillary rise, different volumes will translate into different final heights. After the post-curing step (Fig. 1f), which "freezes" the shape of the final structures, they can be characterized by SEM and AFM.

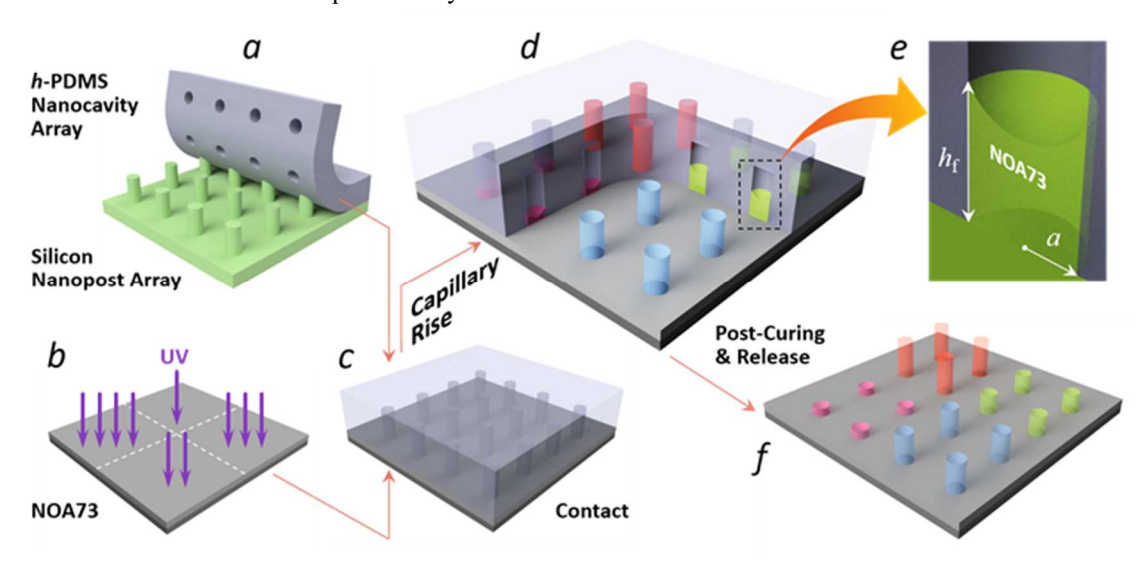


Figure 1: Steps to "freeze-frame" the progress of polymeric capillary rise in nanocavities photofluidically. (a) Preparation of PDMS nanocavities, (b) Preparation of photopolymer thin film with spatially modulated UV pre-curing, (c) Their mutual contact induces (d) Volume-limited capillary rise. (e) The final height (hi) is determined by the UV-dose. (f) After UV post-curing, which "freezes" the photopolymer, the final height can be measured by SEM and AFM.

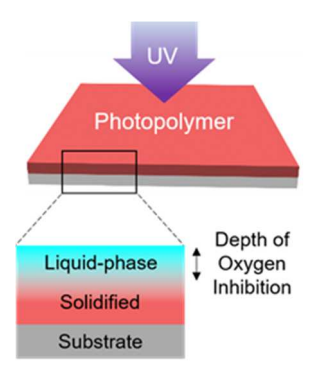


Figure 3: The state of photopolymer under UV precuring. Solidification starts from the inner volume, <u>not</u> the top surface, due to the oxygen inhibition effect.

# **EXPERIMENTAL RESULTS**

# **Accuracy of Optical Freeze-Framing**

Figures 3 and 4 show the result of the optical freezeframing experiments. In principle, the final capillary rise height ( $h_f$  in Fig. 1e) should be inversely proportional to the UV-dose as UV pre-curing reduces the polymer volume available for the capillary action. The relation, obtained from AFM scans, is plotted in Fig. 3. It is clear that the inverse-proportionality is faithfully realized in the experiment. Equally important is the robust nature of the optical freeze-framing process. For each value of UV-dose, at least 10 samples were fabricated and their statistical data were plotted in Fig. 3. The range was as narrow as 3 nm, with its maximum at around 8 nm, endowing the optical freeze-framing technique a sub-10 nm accuracy. The 25-75% range, plotted as the box in the plot, was even narrower. Such a robustness adds reliability to the technique, paving the way to its industrial utilization in future.

In parallel, the accuracy and robustness also assure that the technique is very useful to "capture" the physical picture of the capillary action as a function of the capillary rise height. To that end, in addition to AFM, we have also applied SEM to some of the completed samples. The results are shown in Fig. 4, along with the AFM scans for easy comparison. The SEM images confirm that the capillary action faithfully reproduced the shape of the original nanocapillary without noticeable deformation. The only noticeable deviation from a perfect cylindrical shape was the appearance of the dimples at the top due to the meniscus formation.

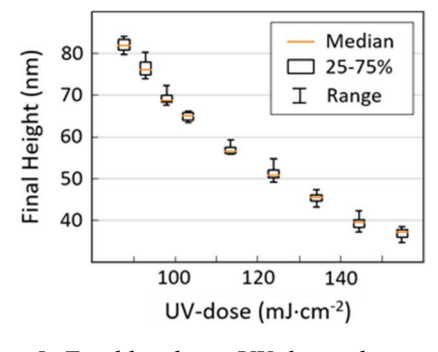


Figure 5: Final height vs. UV-dose relation – The statistics confirms sub-10-nm-scale accuracy in the photofluidic freeze-framing.

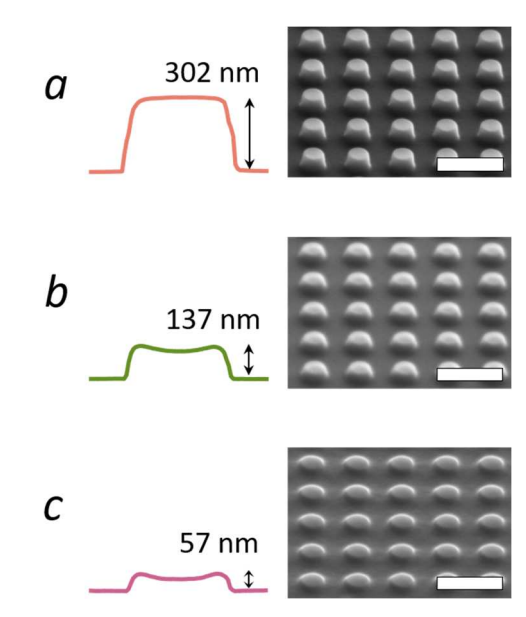


Figure 2: AFM scans and SEM images of photopolymer nanostructures realized with UV-dose of (a) 30, (b) 50, and (c) 110 mJ/cm² (scale bar: 1 µm). The inverse-proportionality between the UV-dose and the final height is clearly shown.

#### **Instability in Nanocapillary Rise**

Figure 5 shows the relation between the UV-dose and the final height over the whole extent of the UV-dose range. The plotted result exhibits an anomaly which defies the volume-control model. At the low-dose regime where the dose is  $< 50 \text{ mJ/cm}^2$ , the value of  $h_f$  jumps abruptly, leaving a forbidden gap in the achievable  $h_f$  value. Such an instability cannot be explained by the purely volume-controlled model which predicts a smooth and continuous height increase. Since this anomaly limits the optical freeze-framing scheme's utility, we investigated its origin. Instabilities in the capillary rise are typically attributed to shear-thinning or elasto-capillarity. NOA73, however, does not exhibit shear-thinning. Elasto-capillarity requires significant capillary deformation, which was not observed in the nanoposts' SEM images (Fig. 4).

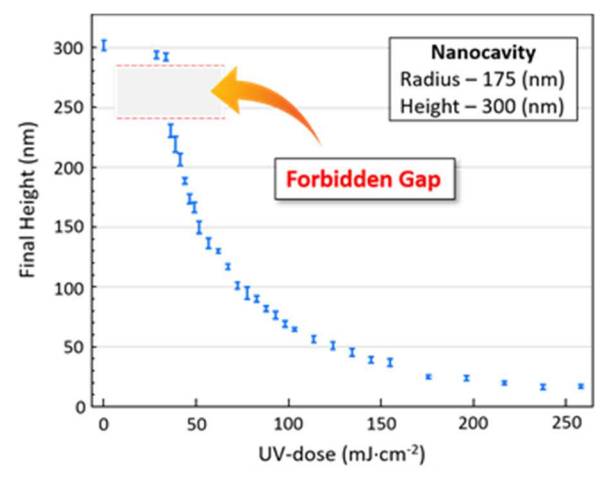


Figure 4: The zoomed-out view of the final height vs. UV-dose relation reveals that the photopolymer's capillary rise is not a linear or gradual process. A sudden jump appears in the final height, leaving a "forbidden gap"

## MODELING AND ANALYSIS

So, we hypothesized that the organic molecules from the partially cured photopolymer, once sorbed on the h-PDMS surface, can plasticize it, increasing its permeability not only to the organic molecules themselves but also to the trapped air molecules [2]. To test the hypothesis, we set up a quantitative model of the plasticization process. Since the affinity of the already sorbed elastomer surface is much higher than that of the pristine surface, the sorption-assisted air-permeation process amplifies itself, relating  $n_{\rm s}$ , the number of the permeated molecules, to the vapor's partial pressure P through  $dn_{\rm s} = K \cdot n_{\rm s}$  dP, where K is a proportionality factor.<sup>5</sup>

For a cylindrical nanocavity undergoing capillary rise, we can rewrite the relation in terms of r as

$$\frac{dn_{s}}{dr} = K \cdot (1 - q \cdot r)^{-1} \cdot (1 - r)^{-2} \cdot n_{s} \tag{1}$$

where  $q = (2h_0)/((a+2h_0))$ ,  $r = h/h_0$ , h = instantaneous capillary rise height, a = nanocavity radius,  $h_o = \text{nanocavity}$  height,  $n_s = \text{the number of permeated molecules}$ . The second and third factors represent the decrease in the nanocavity's surface area and the increase in P due to the capillary rise, respectively. Obviously, the growth of  $n_s$  accelerates as r approaches 1. Its analytical solution is:

$$n_{s}(r) = n_{so} \cdot \left(\frac{1-r}{1-q \cdot r}\right)^{\frac{Kq}{(1-q)^{2}}} \cdot \exp\left(\left(\frac{K}{1-q}\right) \cdot \left(\frac{r}{1-r}\right)\right)$$
(2)

where  $n_{so}$  is the initial value of  $n_s$  at r=0. As shown in Fig. 6, the solution exhibits two regimes. At first, the permeation level stays low, allowing the nanocavity to function as an air-impermeable capillary. Beyond a certain threshold height  $h_t$ , however, it rises very rapidly, rendering h-PDMS "virtually" air-permeable. We specified  $h_t$  as  $h_o \cdot (r_{50} - (r_{100} - r_{50})) = h_o \cdot (2 \cdot r_{50} - r_{100})$  where  $r_{50}$  and  $r_{100}$  are the r levels when  $r_{50}$  equals  $r_{50} = r_{50}$  and  $r_{50} = r_{50}$ . The nanocavity's geometry strongly affects  $r_{50} = r_{50}$  and  $r_{50} = r_{50}$ .

To test the hypothesis, we determined K by matching the computed  $h_t$  to the observed  $h_s$ , and then checked whether that K produces good agreements with the results of other samples universally. To account for the differences in the nanocavity's initial surface areas, K was further scaled by  $S_{\rm ref} / S_{\rm o}$  where  $S_{\rm ref}$  and  $S_{\rm o}$  represent the total

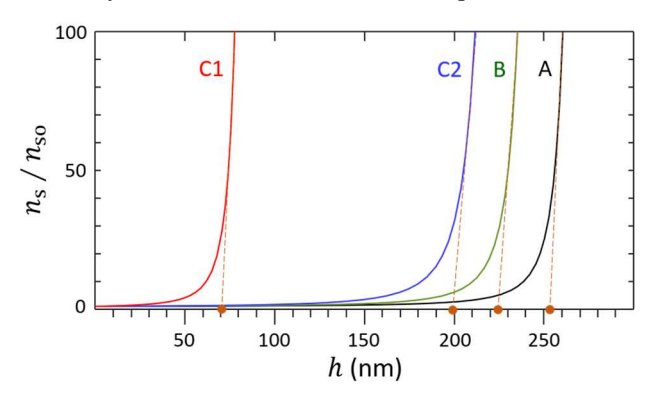


Figure 6: Analytical solutions of Eq. (1) with the threshold values ( $\mathbf{h}_{t}$ ) marked on the  $\mathbf{h}$ -axis.

surface areas of the reference and target nanocavities, respectively. As shown in Fig. 6 and Table 1, the computed  $h_t$  values agreed well with their measured  $h_s$  values, supporting our hypothesis of "virtual air-permeability."

Table 1: Characteristics of the cylindrical nanocavity samples (a: radius,  $\Lambda$ : pitch,  $h_o$ : height,  $h_s$ : observed instability onset height) and the computed instability threshold height  $h_t$ .

Sample	a (nm)	Λ (nm)	h <sub>o</sub> (nm)	h <sub>s</sub> (nm)	h <sub>t</sub> (nm)
A	175	700	300.6±3.2	230.6±3.6	255
В	130	700	286.6±6.6	223.1±1.3	Reference
C1	82.5	600	118.5±2.6	43.5±0.9	71
C2			283.0±3.9	195.3±2.9	199

# APPLICATION FOR NANOPRINTING

Controlling CFL with light is advantageous since light can be 2D-patterned with microscale resolutions through spatial light modulation, unlike other factors previously exploited to control the capillary action, such as annealing time or mechanical pressure. We exploited this beneficial property to extend the light-controlled CFL into spatially resolved grayscale printing of nanopixels.

As the spatial light modulator, we adopted a 10.8  $\mu m$ -pitch micromirror array. It can individually turn on and off the micromirrors at up to 30 kHz. We first directed a collimated UV-light onto the micromirror array to spatially modulate its reflection level (Fig. 7). We could precisely control the time-averaged dose of the UV-reflection from each micromirror using pre-programmed ON/OFF time sequences.

A microscope objective reduced the 2D UV-pattern approximately by a factor of 4, downscaling the minimum feature to a  $2.7\times2.7~\mu\text{m}^2$  pixel. It approximately corresponds to a  $4\times4$  nanopost array in our current samples with  $600\sim700$  nm in pitch. We aligned the lattice direction of the h-PDMS mold along the UV-pixel's orientation using micrometer-actuated opto-mechanical stages. The subsequent CFL steps were the same as before.

We chose sample A as the target and tested two 2-level patterns on it. The first is the checkerboard pattern shown in Fig. 7. We assigned a  $2\times 2$  mirror array to each tile. The resulting tile size was  $5.4\times 5.4~\mu m^2$  which accommodated  $8\times 8$  nanoposts approximately.

The UV-doses of the dark and bright tiles in Fig. 4d are 0 and 90 mJ·cm<sup>-2</sup> which correspond to hf = 300 and 70 nm. The top-view AFM image of the resulting nanopost array (Fig. 7) clearly show that the difference in the UV-dose was successfully translated into the spatially resolved modulation of the nanoposts' height with the modulation depth at approximately 120 nm.

Note that the modulation depth is lower than that expected from Fig. 4 which is approximately 230 nm between 0 and 90 mJ·cm<sup>-2</sup>. The discrepancy is due to the imperfect collimation of the UV-light adopted for the experiment. When the UV-light's etendue is larger than that of the micromirror, the reflection becomes leaked from

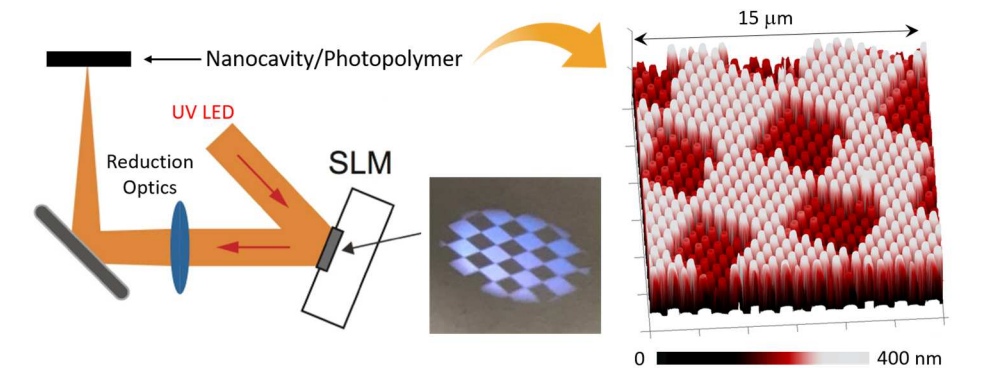


Figure 7: The freeze-framing technique can also be utilized for nanoprinting of nanopillars with different heights by incorporating spatial light modulation (SLM). Microscale resolution can be achieved.

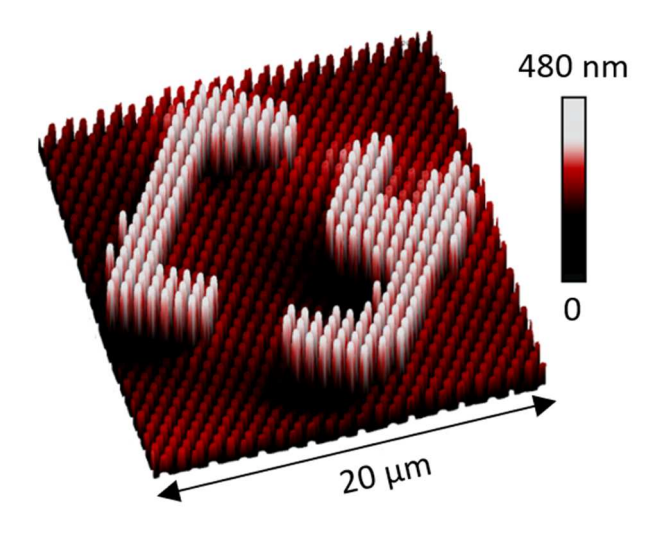


Figure 8: One exemplary result of "nanoprinting" based on the optical freeze-framing technique. Two alphabet characters were "written" within a 20×20  $\mu$ m<sup>2</sup> area optically.

the target area, making the UV-intensity in the bright (dark) area lower (higher) than that reflected from an array of ON (OFF) state micromirrors. The spatial pattern can be further diversified and customized as shown in Fig. 8 in which the alphabet characters "C" and "Y" were "nanoprinted" optically.

## **CONCLUSION**

In conclusion, we have demonstrated nanoscale optical control of photopolymer's capillary rise into elastomeric nanocavities. Using the technique, we observed a variety of interesting phenomena such as the instability in the capillary rise, the formation of a forbidden gap, and the emergence of virtual air-permeability. By exploiting the "freeze-frame" capability of our height-control scheme, we investigated the phenomena in detail and established theoretical models that can enhance our understanding of the nanoscale capillary effect.

# **ACKNOWLEDGEMENTS**

This work was supported by the National Science Foundation under grants CMMI-2129796 and CBET-1605275.

# **REFERENCES**

- [1] K. Y. Suh, Y. S. Kim, and H. H. Lee, *Advanced Materials*, 13 (2001), pp. 1386-1389.
- [2] Kentish, S. E. Polymeric Membranes for Natural Gas Processing. In Advanced Membrane Science and Technology for Sustainable Energy and Environmental Applications; Basile, A.; Nunes, S. P., Eds.; Woodhead Publishing Series in Energy; Woodhead Publishing: Cambridge, MA, 2011; pp. 339–360.

## **CONTACT**

\*Jaeyoun Kim, plasmon@iastate.edu